JOURNAL OF GEOPHYSICAL RESEARCH, VOL. 102, NO. B10, PAGES 22,781–22,797, OCTOBER 10, 1997

SKS splitting beneath continental rift zones

S. Gao,[1] P. M. Davis, H. Liu,[2] P. D. Slack, and A. W. Rigor
Department of Earth and Space Sciences, University of California, Los Angeles

Y. A. Zorin, V. V. Mordvinova, V. M. Kozhevnikov, and N. A. Logatchev
Institute of the Earth's Crust, Siberian Branch, Russian Academy of Sciences, Irkutsk

Abstract. We present measurements of SKS splitting at 28 digital seismic stations and 35 analog stations in the Baikal rift zone, Siberia, and adjacent areas, and at 17 stations in the East African Rift in Kenya and compare them with previous measurements from the Rio Grande Rift of North America. Fast directions in the inner region of the Baikal rift zone are distributed in two orthogonal directions, NE and NW, approximately parallel and perpendicular to the NE strike of the rift. In the adjacent Siberian platform and northern Mongolian fold belt, only the rift-orthogonal fast direction is observed. In southcentral Mongolia, the dominant fast direction changes to rift-parallel again, although a small number of measurements are still rift-orthogonal. For the axial zones of the East African and Rio Grande Rifts, fast directions are oriented on average NNE, that is, rotated clockwise from the N-S trending rift. All three rifts are underlain by low-velocity upper mantle as determined from teleseismic tomography. Rift-related mantle flow provides a plausible interpretation for the rift-orthogonal fast directions. The rift-parallel fast directions near the rift axes can be interpreted by oriented magmatic cracks in the mantle or small-scale mantle convection with rift-parallel flow. The agreement between stress estimates and corresponding crack orientations lends some weight to the suggestion that the rift-parallel fast directions are caused by oriented magmatic cracks.

1. Introduction

A recent review of polarization anisotropy measured on the continents [*Silver*, 1996] concludes that in transpressive regions anisotropy is caused by vertically coherent deformation of the mantle with fast directions parallel to the compressional features. While this behavior is observed for compressive regions such as the Alps, Tibet, and the Tien Shan, the same process operating in regions of extension is expected to generate fast directions parallel to the extension. Contrary to this expectation, we present results from three continental rift zones, the Rio Grande Rift (RGR), the Baikal rift zone (BRZ) and the East African Rift (EAR) where fast directions are observed orthogonal to the extension. We propose that a plausible explanation for these observations is that in regions of mantle extension, of high heat flow, and of volcanism, magma-filled oriented cracks in the mantle can give rise to the observed polarization.

Polarization anisotropy determined by SKS splitting is developing as a tool to examine finite strain caused by flow in the uppermost mantle [*Fuchs*, 1977; *Ando et al.*, 1983; *Silver and Chan*, 1988, 1991; *Vinnik et al.*, 1989, 1992; *Savage et al.*, 1990; *Silver*, 1996]. The earliest indications that seismic anisotropy is related to mantle flow were observations of fast mantle velocities perpendicular to mid-ocean ridges [*Hess*, 1964; *Raitt et al.*, 1969; *Forsyth*, 1975]. Azimuthal dependence of velocities of long-period Rayleigh waves has been observed by *Tanimoto and Anderson* [1985] and *Montagner and Tanimoto* [1991], who noted that the global map of fast phase velocities correlates with absolute plate motions. Subsequently, numerous observations have been made of SKS splitting in diverse tectonic settings (see reviews by *Vinnik et al.* [1992] and *Silver* [1996]). *Vinnik et al.* [1992] report single station measurements from rift zones such as the Red Sea rift, the Baikal rift, the continental extension of the Arctic ridge, and the Rhinegraben. They conclude that in regions of rifting, the inferred directions of flow in the mantle from the SKS fast directions are close to the extension directions in the crust. However, for the Rio Grande and the French Massif Central, they find that the fast directions are ori-

[1]Now at Department of Terrestrial Magnetism, Carnegie Institution of Washington, D.C.

[2]Also at Department of Terrestrial Magnetism, Carnegie Institution of Washington, D.C.

Paper number 97JB01858.
0148-0227/97/97JB-01858$09.00

ented nearly 50° to the direction of extension. Recent measurements of near ridge splitting in Iceland [*Bjarnason et al.*, 1996] give fast directions that are closer to parallel to the ridge than perpendicular to it. In this paper we examine about 80 continental rift zone measurements in order to address further the question whether in regions of continental extension fast directions are parallel or perpendicular to the extension direction.

SKS splitting can be used to characterize seismic anisotropy beneath a seismic station [e.g., *Kind et al.*, 1985; *Silver and Chan*, 1988, 1991; *Vinnik et al.*, 1989; *Savage et al.*, 1990; *Makeyeva et al.*, 1992; *Silver and Kaneshima*, 1993; *Gao et al.*, 1994a; *Liu et al.*, 1995; *Gao*, 1995; *Silver*, 1996]. The azimuthal anisotropy of the mantle is readily detected by birefringent effects on *SKS* phases from earthquakes with epicentral distance greater than 85°. The *SKS* phase travels as an *S* wave in the crust and mantle and as a *P* wave through the liquid outer core. At the core-mantle boundary on the receiver side, the *S* wave is radially polarized. If this shear wave encounters anisotropic material on its path to the receiver, it may split into two different polarizations having different velocities denoted fast and slow. The splitting parameters are the polarization of the fast split shear wave ϕ (measured clockwise from the north) and the travel time difference between the fast and slow shear waves δt. The method used to calculate the optimal splitting parameters and their standard deviations was described extensively by *Silver and Chan* [1991].

It is generally believed that the main cause for *SKS* splitting in the mantle is the lattice preferred orientation (LPO) of crystallographic axes of elastically anisotropic minerals in the upper mantle [e.g., *Hess*, 1964; *Francis*, 1969; *Karato*, 1989; *Savage et al.*, 1990; *Babuska and Cara*, 1991; *Silver and Chan*, 1991; *Chastel et al.*, 1993; *Silver*, 1996]. Both olivine and orthopyroxene are highly anisotropic upper mantle constituent minerals. Mantle peridotites typically contain more than 65% olivine and 20% orthopyroxene [*Anderson*, 1989]. Since orthopyroxene is not as abundant and anisotropic as olivine, it is generally assumed that the upper mantle beneath a station is composed of a certain percentage of oriented olivine. The rest is assumed to be randomly oriented olivine, orthopyroxene, and other mantle minerals. It must be mentioned that in reality the alignment of orthopyroxene may reduce overall anisotropy caused by olivine alignment, since its fast axis doesn't align parallel to olivine fast axis during deformation [*Christensen and Lundquist*, 1982].

For an individual olivine crystal, the fastest *P* wave propagation direction is along the *a* axis with $V_a = 9.87$ km/s; along the *b* axis the *P* wave has the slowest velocity with $V_b = 7.73$ km/s; and along the *c* axis the *P* wave has the intermediate velocity with $V_c = 8.65$ km/s [*Verma*, 1960]. The fastest *S* waves are those polarized along the *a* axis. *McKenzie* [1979] assumed that under sufficiently high stress and finite strain, seismic anisotropy in peridotites is controlled by finite strain with the *a*, *b*, and *c* axes of olivine becoming aligned with the longest, shortest, and intermediate axes of the finite strain ellipsoid. *McKenzie*'s [1979] approach was pursued by *Ribe* [1992] who developed orientation distribution formulas for deformation-induced LPO of *Ribe and Yu* [1991]. According to the theory, under uniaxial compression, the *a* axis of olivine turns to be perpendicular to the maximum compressional strain direction; under pure shear, it becomes perpendicular to the shortening direction; and under progressive simple shear, it aligns in the flow direction. This interpretation has been supported by numerous observations of anisotropic textures in deformed mantle rocks complemented by measurements and theoretical estimates of their seismic anisotropy [*Hess*, 1964; *Crosson and Lin*, 1971; *Christensen*, 1971, 1984; *Baker and Carter*, 1972; *Nicolas et al.*, 1973; *Peselnick et al.*, 1974; *Christensen and Salisbury*, 1979; *Christensen*, 1984; *Mercier*, 1985; *Nicolas and Christensen*, 1987; *Silver and Chan*, 1991; *Chastel et al.*, 1993].

A continental rift is defined as an elongated topographic depression overlying a place where the entire lithosphere has been significantly modified in extension [*Olsen and Morgan*, 1995]. In continental rift zones we would expect that if the entire lithosphere is extended the *a* axes and therefore the splitting fast directions would cluster in the direction of rift opening. Some common features of a typical continental rift zone include (1) the central part of rift valley subsides and the edges of the adjacent blocks are uplifted; (2) flanking normal faults; (3) negative Bouguer gravity anomalies; (4) higher than normal heat flow; (5) shallow, tensional and higher than normal seismicity; and (6) thinning of the crust beneath the rift valley [*Turcotte and Schubert*, 1982; *Fowler*, 1990]. All these features mark the initial stages of continental breakup where the lithosphere pulls apart and upwelling hot mantle rises beneath the spreading rift to eventually form oceanic lithosphere and an ocean basin.

The mechanisms of continental rifting can be separated into two end-members called passive and active rifting. For passive rifting the entire lithosphere extends beneath the rift zone. For this case, LPO is expected to align in the direction of extension. Active rifting involves erosion of the lithosphere by mantle convection causing the asthenosphere to upwarp beneath the rift axis. If a fabric develops in the asthenosphere, its direction will depend on the details of the convection. Two mechanisms for the development of anisotropy in upwelling asthenosphere have been considered by *Kendall* [1994] for the mid-ocean ridge case. The first involves the preferential alignment of fast axes of olivine crystals; the second involves preferentially aligned magma-filled cracks.

We compare *SKS* and tomographic measurements from the three major Cenozoic continental rift areas (Figure 1): the Rio Grande Rift (RGR) of North America [*Sandvol et al.*, 1992], the East African Rift (EAR)

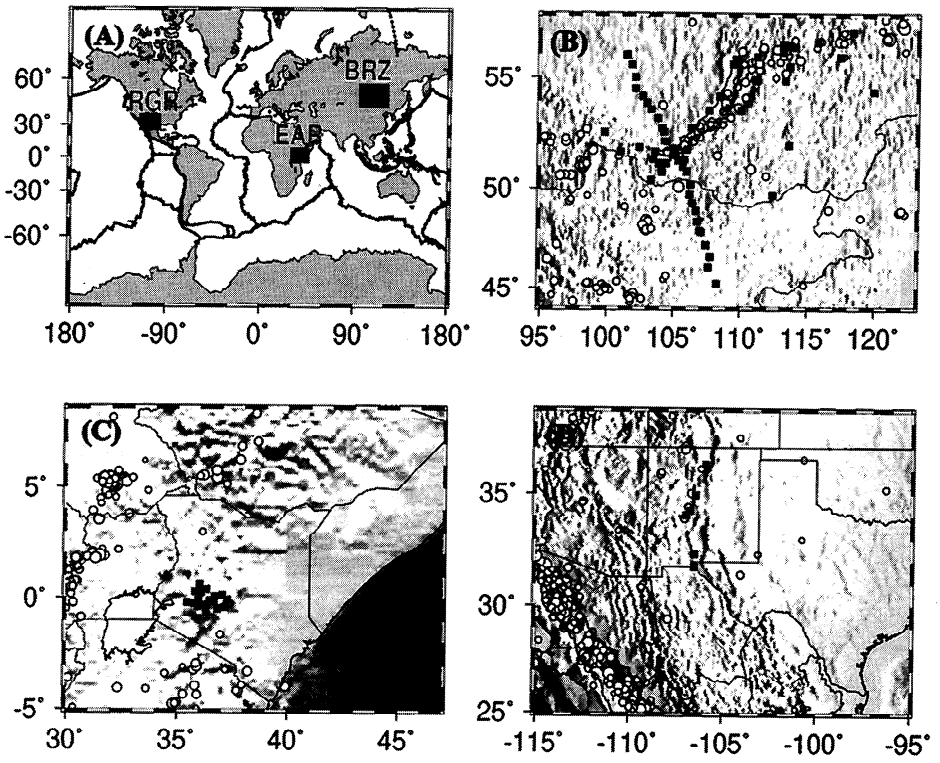

Figure 1. Mercator projection maps showing locations of the three rifts and their topography and seismicity. (a) Locations of the 3 rifts on a global map; (b)–(d) Stations used in the study (solid squares), location of $M_b \geq 4.5$ earthquakes that occurred 1965–1992 (open circles), and topography for Baikal rift zone, East African Rift, and Rio Grande Rift, respectively. The geographic areas in Figures 1b, 1c, and 1d have approximately the same dimensions.

[*Gao et al.*, 1994c], and along a 1280 km profile across the Baikal rift zone (BRZ) using the data from a portable experiment [*Gao et al.*, 1994a; *Gao*, 1995] along with new estimates from data provided by the Baikal Seismic Network.

2. Data and Results

2.1. Baikal Rift Zone (BRZ)

In this section we extend our previous *SKS* splitting results [*Gao et al.*, 1994a] to include a data set that we recently collected from the permanent seismic array operated in the Baikal rift zone.

2.1.1. Data. Station locations are shown in Figure 2 and listed in Table 1. We separated the region into six subareas which approximately correspond to the major tectonic provinces of the area. Lake Baikal sits on the southeast margin of the Siberian craton in a region that underwent collisional tectonics in the Mesozoic followed by regional extension in the Cenozoic. To the south lies the Mongolian fold belt, a region of transpression thought to be related to the collision of India with Asia. Areas A, B, and C comprise the BRZ with area A including the NE rift valleys, area B including the central rift valleys, and area C including the southern rift valleys; area D is the Siberian platform, area E is the northern Mongolian fold belt, and area F is the southern Mongolian fold belt. The stations within an area are numbered from north to south, e.g., the northernmost station in area A is A01 and the southernmost one is A11.

The 63 stations belong to two seismic networks. Stations named 92xx in Table 1a were from a portable Program for Array Seismic Studies of the Continental Lithosphere (PASSCAL) experiment conducted in the summer of 1992 by a field team from the Institute of Earth's Crust (IEC), Irkutsk, University of Wisconsin (UW), and University of California, Los Angeles (UCLA). *SKS* splitting parameters on most of these sites were previously reported [*Gao et al.*, 1994a]. The remaining stations with alphabetical names such as "boda" belong to the Baikal Seismic Network operated by IEC. For this study the analog seismograms were scanned and digitized using the NXSCAN software package [*Humphrey and Helmberger*, 1993]. Locations of the 31 events used in the analysis are shown in Figure 3, and event information is listed in Table 2.

Figures 4 and 5 show original *SKS* signals before and after correction for splitting along with their particle motion patterns at station E01 for two events. One of the evnets (event 8) exhibits excellent splitting, the other (event 17) does not. When the difference between the radial direction of an event-station pair and fast *SKS* direction is near 0° or 90°, the anisotropy effect

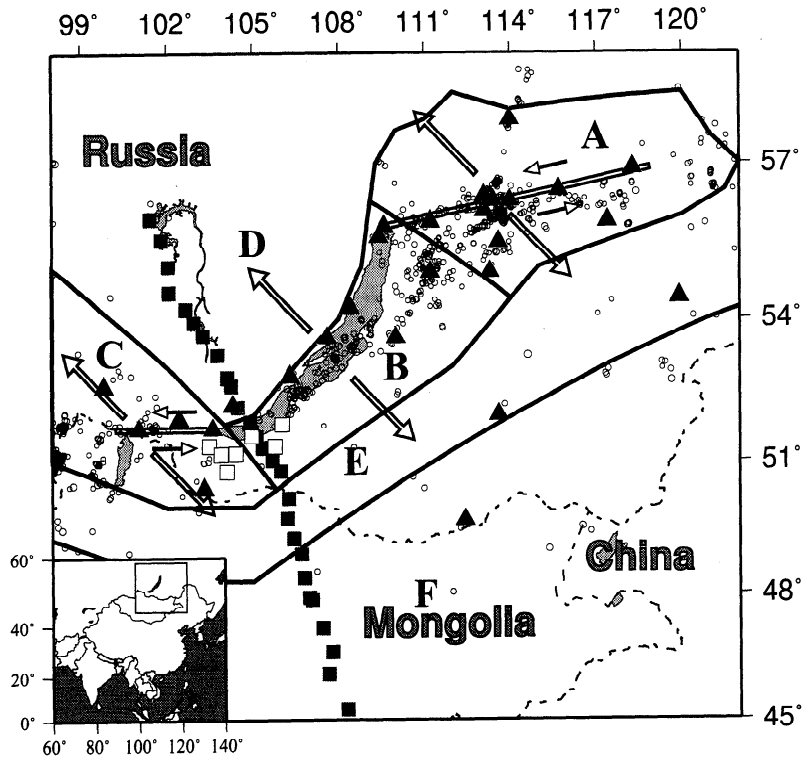

Figure 2. A Mercator projection map for the Baikal-Mongolia area showing locations of stations used in the study, regional stress fields associated with BRZ, and local events that occurred during the field experiment (open cirlcles). Triangles are Baikal Seismic Network analog stations, and squares are digital stations operated in the summer of 1992. Solid squares represent stations with previous *SKS* splitting measurements [*Gao et al.*, 1994a]. Arrows show regional stress fields of the Baikal rift zone obtained from surface geological structure analysis and earthquake focal mechanism studies [*Sherman*, 1992]. The study region is divided into six areas: areas A, B, and C are the Baikal rift zone which is outlined by the thick gray lines. Area A is the NE part of the BRZ, area B is the main rift zone, and area C is the SW part of the BRZ. Area D is located on the Siberian Platform, area E is the northern Mongolian fold belt, and area F is located on the Mongolian fold belt. The lower left inset shows coastlines and national borders of Asia and the location of the study area.

cannot be observed and the measurement is null [*Silver and Chan*, 1991]. Three nondistinguishable possibilities may apply in such a case: the upper mantle beneath the station is (1) isotropic; (2) anisotropic with an unknown splitting time and a fast direction parallel to the radial direction; and (3) anisotropic with an unknown splitting time and a fast direction perpendicular to the transverse direction. As demonstrated in Figures 4 and 5, if only event 17 were available, the result from station E01 would be a null measurement. The availability of event 8, which is from a different azimuth, resolves the measurement.

2.1.2. Results. The final results of *SKS* splitting measurements (Figure 6 and Table 1a) were obtained by weighted averaging according to the 95% confidence interval of each individual measurement. The splitting ranges from 0.3 to 2.1 s which could have been caused by layers of 30 to 210 km thick, respectively, characterized by 4% anisotropy. Although directions in the vicinity of the BRZ appear to be randomly distributed, examination of the scatter reveals some trends. Figure 7 shows normalized rose diagrams of the fast directions for the six areas. The rose diagrams indicate that there are two dominant directions. One of the directions is about $60° \pm 20°$, which is approximately parallel to the strike of the surface expression of the BRZ as well as the strike of the upper mantle low-velocity structure inferred from travel time inversion [*Gao*, 1995]. The second direction is about $140° \pm 20°$, which is approximately orthogonal to the rift axis.

2.1.2.1. Area A: The peak values on the rose diagram for this area are 60° for the rift-parallel group and 130° for the rift-orthogonal group. Of the 11 stations in this area, two (A03, A10) have null measurements. Three of the four stations (A05, A06, A07, A08) in the rift-parallel group are located in the middle part of this area. The two stations which belong to the rift-orthogonal group are located near the northern boundary (A01) and on the southern boundary (A11).

2.1.2.2. Area B: Most of the stations with null measurements are located within this area. Five stations (B01, B02, B07, B12, and B15) near the rift axis

Table 1a. *SKS* Splitting Measurement Results in the Baikal Rift Zone

Station	Station Name	Coordinates		Fast Direction, deg	Splitting Time, s	Number of Events
		Latitude, deg	Longitude, deg			
A01	boda	57.800	114.000	136.0±13.0	0.70±0.50	2
A02	char	56.900	118.300	107.9± 6.0	0.82±0.24	2
A03	nely	56.500	115.700	29.0± —	—	3
A03	nely	56.500	115.700	119.0± —	—	3
A04	turi	56.400	113.100	86.0±24.0	0.80±0.50	1
A05	ozer	56.300	114.000	49.0± 7.0	0.70±0.30	1
A06	tonn	56.300	113.400	64.0± 8.0	1.40±0.30	1
A07	kovo	56.100	113.100	57.0± 9.0	0.80±0.30	1
A08	kala	55.900	117.400	61.0±35.0	0.50±0.30	1
A09	kumo	55.900	111.200	161.0±24.0	0.70±0.50	1
A10	uaki	55.500	113.600	38.5± —	—	3
A10	uaki	55.500	113.600	128.5± —	—	3
A11	tsip	54.900	113.300	120.0± 6.0	1.40±0.90	1
B01	nizh	55.800	109.600	41.3± 3.2	0.84±0.19	5
B02	sbai	55.600	109.400	46.0±50.0	0.30±0.20	1
B03	ulun	54.900	111.200	76.0±20.0	0.60±0.30	1
B04	solo	54.200	108.400	26.0± —	—	1
B04	solo	54.200	108.400	116.0± —	—	1
B05	ongu	53.600	107.600	21.0± —	—	2
B05	ongu	53.600	107.600	111.0± —	—	2
B06	suvo	53.600	110.000	82.0±35.0	0.40±0.30	1
B06	suvo	53.600	110.000	15.2± 5.5	1.80±0.64	2
B07	tyrg	52.800	106.300	44.6± 3.3	0.85±0.12	4
B08	9212	51.847	104.893	144.0±19.0	0.60±0.40	1
B09	9250	51.799	106.015	22.0± —	—	1
B09	9250	51.799	106.015	112.0± —	—	1
B10	9233	51.541	104.942	127.0±10.0	0.70±0.30	1
B11	9224	51.526	105.121	148.0±17.0	1.30±0.30	1
B12	9235	51.320	105.761	45.7± 8.7	0.39±0.17	2
B13	9221	51.292	105.339	131.5± 6.3	0.91±0.25	3
B14	9222	51.021	105.682	137.9± 6.2	1.09±0.14	3
B15	9223	50.791	105.970	37.6± 3.8	1.00±0.21	2
B15	9223	50.791	105.970	129.0± 7.0	1.60±0.41	2
C01	orli	52.600	99.800	70.0±10.0	0.80±0.20	1
C01	orli	52.600	99.800	139.6± 4.8	1.00±0.17	3
C02	arsh	51.900	102.400	92.1±11.9	1.18±0.50	2
C03	mond	51.700	101.000	125.5± 2.9	1.48±0.20	4
C04	tala	51.700	103.600	128.7± 4.3	0.82±0.20	5
C05	9270	51.336	103.458	24.0± —	—	1
C05	9270	51.336	103.458	114.0± —	—	1
C06	9272	51.167	104.407	141.0± 7.1	1.10±0.21	2
C07	9271	51.153	103.877	21.0± —	—	1
C07	9271	51.153	103.877	111.0± —	—	1
C08	9237	50.780	104.089	58.8± 5.5	0.83±0.17	2
C09	zaka	50.400	103.300	66.5± 8.3	0.86±0.24	2
C09	zaka	50.400	103.300	127.0±12.0	1.70±0.50	1
D01	9200	55.965	101.410	133.0± 7.0	1.00±0.50	1
D02	9215	55.560	101.803	170.0±13.0	0.90±0.40	1
D03	9213	55.022	102.055	144.8± 3.5	0.82±0.07	5
D03	9213	55.022	102.055	144.8± 3.5	0.82±0.07	5
D04	9203	54.516	102.070	127.5± 3.7	1.18±0.12	9
D05	9204	54.193	102.649	143.8± 2.6	0.72±0.09	7
D06	9205	53.929	102.934	149.2± 8.9	0.58±0.15	3
D07	9206	53.649	103.255	20.0± —	—	5
D07	9206	53.649	103.255	110.0± —	—	5
D08	9207	53.243	103.767	20.0± —	—	2
D08	9207	53.243	103.767	110.0± —	—	2
D09	9209	52.778	104.105	137.7± 4.8	0.90±0.16	3
D10	9210	52.622	104.234	138.2± 7.4	0.60±0.13	6
D11	irku	52.200	104.300	25.0± —	—	2
D11	irku	52.200	104.300	115.0± —	—	2
D12	9211	52.169	104.469	20.0± —	—	4
D12	9211	52.169	104.469	110.0± —	—	4

Table 1a. (continued)

Station	Station Name	Coordinates		Fast Direction, deg	Splitting Time, s	Number of Events
		Latitude, deg	Longitude, deg			
E01	tupi	54.400	119.900	101.0± 8.0	0.90±0.30	1
E02	chit	52.000	113.600	30.0± —	—	9
E02	chit	52.000	113.600	120.0± —	—	9
E03	9280	50.193	106.254	137.0±16.0	1.50±0.40	1
E04	9291	49.747	106.188	145.3±16.0	0.78±0.14	4
E05	9282	49.738	106.202	147.2±23.5	0.34±0.30	2
E06	9283	49.288	106.412	134.1± 9.0	0.37±0.16	4
F01	hapc	49.700	112.400	71.2± 7.2	0.62±0.15	3
F02	9284	48.931	106.682	39.1±10.9	1.04±0.39	2
F02	9284	48.931	106.682	132.0± 9.9	0.84±0.57	2
F03	9285	48.383	106.783	105.2± 5.9	1.13±0.26	4
F04	9286	47.921	106.954	64.4± 4.5	0.75±0.14	3
F05	9292	47.866	107.051	69.2± 6.2	0.70±0.13	3
F06	9287	47.209	107.422	44.2± 6.7	0.32±0.08	4
F07	9288	46.635	107.758	56.2± 9.6	0.40±0.14	2
F07	9288	46.635	107.758	132.2± 3.1	1.50±0.19	3
F08	9289	46.115	107.619	54.7±21.8	1.28±0.32	3
F09	9290	45.262	108.260	84.7±34.4	1.42±0.62	5

show rift-parallel fast directions. The peak value on the rose diagram for this area is 50°, which corresponds to the rift-parallel group. Most of the other stations have fast directions orthogonal to the rift axis, as evidenced by the 130° fast direction peak on the rose diagram (Figure 7). The rapid change of the fast directions at stations B12 and B13, which are only 30 km apart, may indicate that the main part of the source of anisotropy in the area is shallow, probably at a maximum depth of less than 50 km, as indicated by the Fresnel zone forward modeling of *Gao* [1995]. If the anisotropy contrast lies significantly deeper than this, the Fresnel zone is broader and the transition in the fast directions would spread out over a longer distance than observed.

2.1.2.3. Area C: The rift-parallel fast directions are not as common as the rift orthogonal ones, as shown in the rose diagram for this area. The most common value for the rift-parallel fast directions is about 60°, and for the rift-orthogonal group it is 130°.

2.1.2.4. Area D: Of the 12 stations in this area, four have null measurements. The rest of the measurements belong to the rift-orthogonal group.

Table 1b. *SKS* Splitting Measurement Results in the East Africa Rift Zone

Station	Coordinates		Fast Direction, deg	Splitting Time, s	Number of Events
	Latitude, deg	Longitude, deg			
K04	-0.19	35.44	20.4± 7.3	0.86±0.21	4
K07	-0.24	35.75	28.5± 8.5	1.43±0.31	2
K09	-0.37	35.92	20.0± 3.0	2.00±0.20	1
K10	0.64	36.01	32.2±10.3	1.55±0.38	2
K12	-0.10	35.94	26.0±12.0	1.50±0.40	1
K15	-0.62	36.30	19.0±30.0	2.40±0.50	1
K16	0.40	36.29	176.0±13.0	0.90±0.40	1
K24	-0.17	36.63	35.0±19.0	1.10±0.70	1
K25	-0.47	36.82	26.4± 8.1	1.24±0.38	2
K31	-0.07	37.25	10.0± 7.0	1.90±0.70	1
K45	0.29	35.80	26.0±12.0	2.30±0.40	1
K47	0.24	36.07	55.0±28.0	1.50±0.80	1
K50	-0.33	36.32	22.0±27.0	1.90±0.90	1
K51	-0.11	36.46	33.0±20.0	1.50±0.40	1
K52	0.06	36.67	43.0±13.0	0.80±0.30	1
K53	0.12	37.02	10.0± 9.0	1.20±0.50	1
K54	-0.40	37.17	172.0± 7.0	0.80±0.30	1

Table 1c. *SKS* Splitting Measurement Results in the Rio Grande Rift Zone

Station	Coordinates		Fast Direction, deg	Splitting Time, s
	Latitude, deg	Longitude, deg		
CZL	36.28	-105.91	26.0	0.9
ANMO	34.95	-106.46	41.0	1.5
SEVI	34.27	-106.73	41.0	1.1
WTX	34.07	-106.95	46.0	1.1
WSMR	32.34	-106.49	11.0	1.2
ELPA	31.77	-106.51	5.0	1.5

From *Sandvol et al.* [1992].

2.1.2.5. Area E: The dominant fast direction is rift-orthogonal. The peak value in the rose diagram for this area is 140°.

2.1.2.6. Area F: The dominant fast directions in this area range from 40° to 80°. The fast direction for the southernmost station is nearly E-W. At the northern part of this area, the transition from the dominant rift-orthogonal fast directions in area E to the dominantly ENE fast directions in this area takes place over a distance of about 50-90 km. Once again, using the result of Fresnel zone forward modeling [*Gao*, 1995], the maximum depth of the source of the anisotropy near this transition is about 200 km.

In Figure 8 we compare the BRZ results with other clustered measurements in Asia. The fast direction for the southern part of the BRZ profile is roughly ENE, which is consistent with the dominant direction found across the Tibetan Plateau [*McNamara et al.*, 1994] and in the Tien Shan area [*Makeyeva et al.*, 1992]. Both the Tibetan and the Mongolian Plateaus and the Tien Shan area have been deformed by Cenozoic deformation related to the collision between the Indian and Eurasian plates. The observed fast directions in these areas may have the same origin, i.e., the recent continental collision [*Gao et al.*, 1994a].

2.2. East African Rift (EAR)

Using data we recorded during the 1989/1990 Kenya Rift International Seismic Project (KRISP) [*Slack et al., 1994*], we found *SKS* arrivals at 17 stations suitable for splitting analysis (Figure 9 and Table 1b). The backazimuth for all of the eight events used in measuring *SKS* splitting lies within a narrow range of 60° to

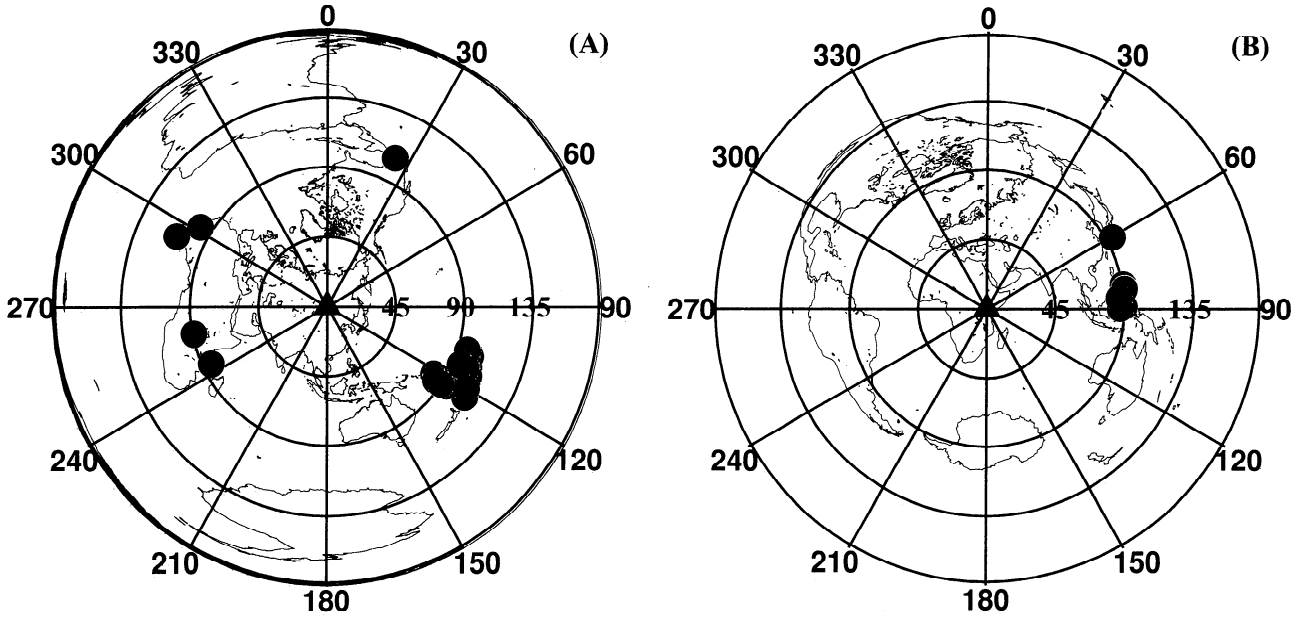

Figure 3. Azimuthal equidistant projection maps showing epicenters of events used in the study of *SKS* splitting for (a) BRZ and (b) EAR. The center of Figure 3a is station B11, and that of Figure 3b is station K12. The three circles represent 45°, 90°, and 135° epicentral distances. Numbers on the periphery indicate azimuths of events relative to the center of map.

Table 2a. Events Used in *SKS* Splitting Studies for the Baikal Rift Zone

Event	Origin			Coordinates		Depth, km	Back azimuth deg	Distance, deg
	Year	Day	Time,UT	Latitude, °N	Longitude, °E			
1	1980	104	1804	-23.466	-177.297	79	114.12	100.71
2	1980	298	1453	18.211	-98.240	72	23.29	107.61
3	1981	187	0308	-22.293	171.742	33	121.58	93.72
4	1982	153	1237	-18.083	-172.492	33	107.16	99.33
5	1983	356	0411	11.866	-13.529	11	299.91	97.68
6	1984	272	0003	-25.849	-175.911	21	114.63	103.35
7	1984	289	1021	-15.860	-173.643	128	106.63	96.92
8	1985	134	1811	-10.562	41.424	10	242.75	82.53
9	1986	146	1906	-20.190	178.860	538	114.96	95.95
10	1986	303	0128	-21.702	-176.616	188	112.51	99.72
11	1987	279	0419	-17.940	-172.225	16	106.87	99.38
12	1988	282	0446	-18.771	-172.415	35	107.54	99.91
13	1988	284	1820	-28.644	-177.553	27	117.61	104.59
14	1989	070	0505	-17.766	-174.761	230	108.67	97.74
15	1990	004	0532	-15.397	-172.850	53	105.74	97.03
16	1990	050	0648	-15.465	166.385	12	121.96	85.26
17	1990	174	2138	-21.568	-176.483	180	112.33	99.70
18	1991	305	1623	-30.255	-177.981	21	118.96	105.60
19	1992	177	0630	-28.063	-176.735	18	116.65	104.60
20	1992	178	0318	-33.682	-179.076	33	121.97	107.65
21	1992	193	1044	-22.284	-178.507	381	114.27	99.09
22	1992	217	0658	-21.584	-177.322	278	112.96	99.22
23	1992	217	2108	-12.023	166.496	109	119.97	82.46
24	1992	238	0824	-20.620	-175.151	67	110.75	99.73
25	1992	241	1715	-22.154	-179.620	597	115.02	98.36
26	1992	241	1818	-0.996	-13.557	10	292.53	108.25
27	1992	243	2009	-17.738	-178.775	573	111.69	95.36
28	1992	254	1043	-22.518	-175.052	39	111.87	101.26
29	1992	255	0357	-6.091	26.680	10	257.19	87.58
30	1992	259	2104	-14.122	167.263	196	120.51	84.61
31	1992	285	1924	-19.276	168.913	157	122.06	89.75

90° (Table 2b). The stations used were distributed in a 400 by 200 km E-W elongated area centered at (36.5°E, 0°N). Most of the stations were within or very close to the rift valley. Fourteen of the 17 stations analyzed have a fast direction of 30 ± 20°, which is subparallel to the N-S striking rift system. Thus fast directions are closer to orthogonal to the extension direction rather than parallel to it, which was expected if the extension has the effect of orienting mantle crystals [*Gao et al.*, 1994c].

2.3. Rio Grande Rift (RGR)

In the RGR study by *Sandvol et al.*, [1992], the six stations used were within or very close to the rift valley. The resulting fast *SKS* polarization directions are NNE, i.e., parallel or subparallel to the rift axis (Figure

Table 2b. Events Used in *SKS* Splitting Studies for the East Africa Rift

Event	Origin			Coordinates		Depth, km	Back azimuth deg	Distance, deg
	Year	Day	Time,UT	Latitude, °N	Longitude, °E			
1	1989	328	0035	0.989	126.007	25	89.0	88.8
2	1989	342	1023	10.094	126.495	43	80.0	91.1
3	1989	343	2038	0.141	123.340	151	89.8	87.6
4	1989	350	0033	8.431	126.942	36	81.6	91.5
5	1989	350	0053	8.396	126.848	29	81.7	91.0
6	1989	354	0835	8.192	126.852	39	81.9	91.0
7	1990	048	0228	29.533	130.732	65	60.6	93.3
8	1990	073	0344	4.575	122.620	639	85.4	86.7

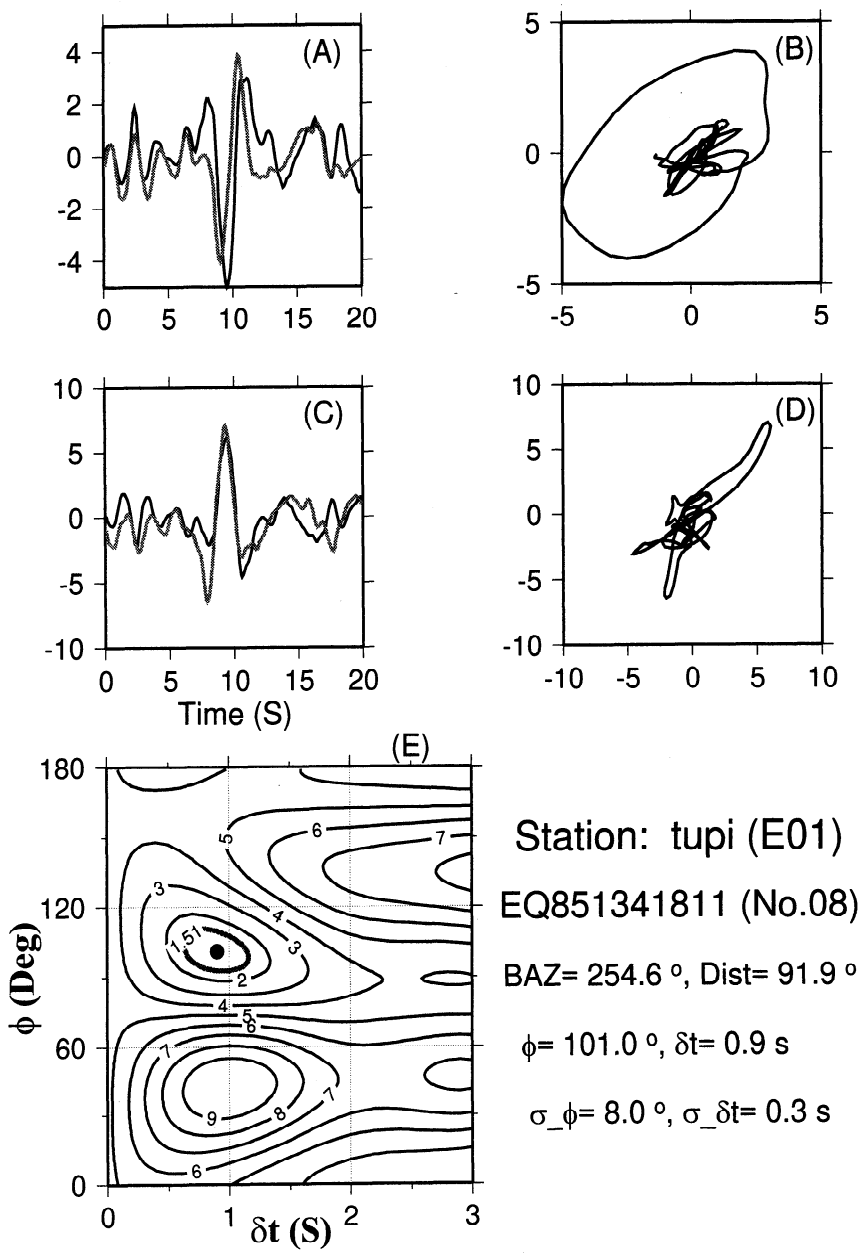

Figure 4. Diagrams showing example data and the procedure for finding the optimal parameters for event 8. (a) the original seismograms of radial (black) and transverse (gray) components, (b) their particle motion pattern, (c) radial and transverse components of corrected seismograms, (d) the particle motion pattern of the corrected components, and (e) the contour map of an error function, the minimum of which corresponds to the optimal parameter pair. The seismograms in Figure 4c were corrected from those shown in Figure 4a using the optimal parameter pair indicated by a dot on Figure 4e. Station and event names, backazimuth (BAZ) and distance (DIST) of the event relative to the station, as well as the optimal parameters and their errors, are indicated at the bottom right. The 95% confidence region is confined by a thick gray contour line in Figure 4e.

10 and Table 1c). The splitting time was found to range from 0.9 to 1.5 s; no measurements were made on the flanks of the rift zone. West of the rift, in California and Nevada, the dominant fast direction is east-west [e.g., *Vinnik et al.*, 1992; *Savage and Silver*, 1993; *Liu et al.*, 1995]. The rift-parallel fast direction was interpreted by *Sandvol et al.* [1992] to result from rift-parallel flow in a small-scale mantle convection cell beneath the rift.

3. Discussion

We had expected to find that rift zones would have fast directions in the extension direction if the mantle beneath the rifts extends, aligning olivine crystals. However, we have found that for the Kenya and Rio Grande Rifts and parts of the Baikal rift zone, fast directions are orthogonal to the extension direction. For

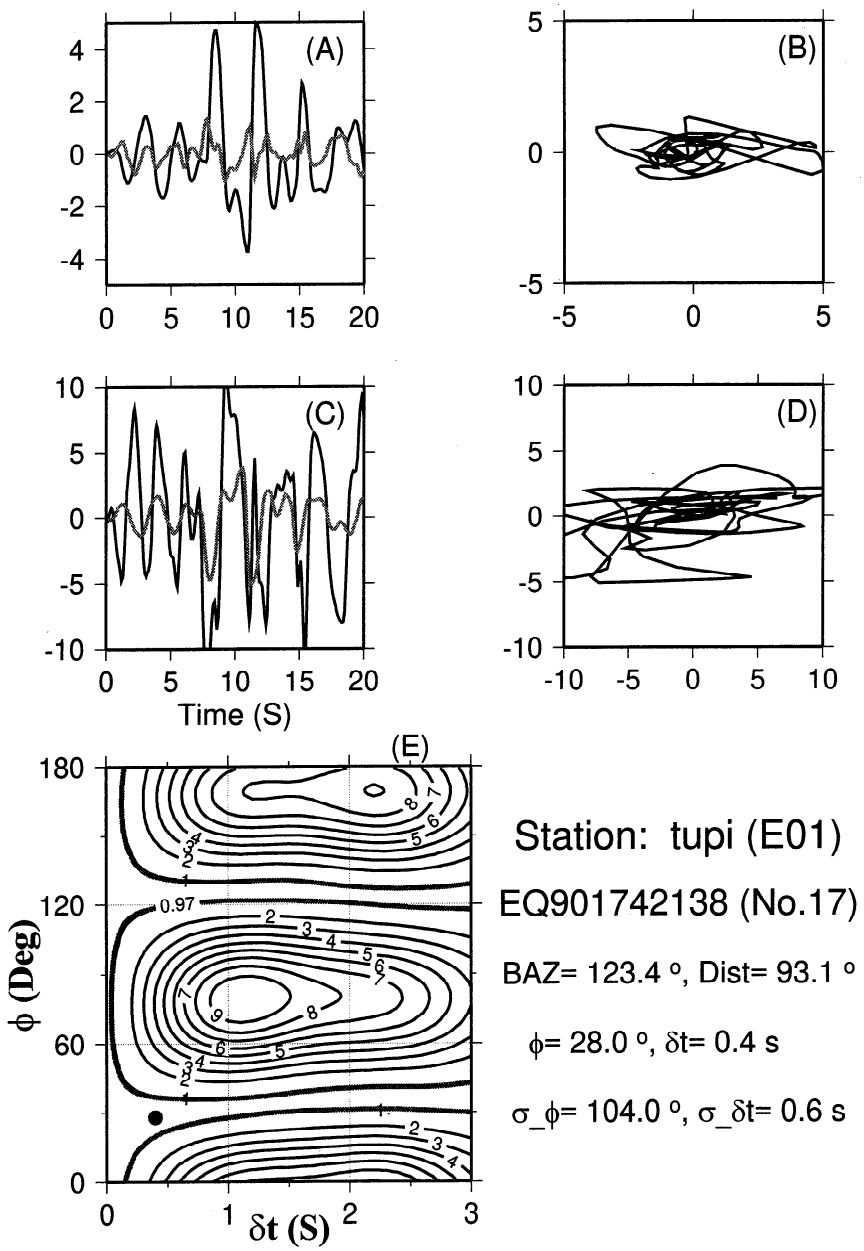

Figure 5. Same as Figure 4, except for event 17.

Baikal, fast directions are found in the rift zone that are both parallel and perpendicular to extension. Interpretation of the *SKS* splitting measurements is difficult in that the anisotropy may be a remnant of past tectonic strain, or caused by mantle flow, or in regions where the mantle is melting, could be caused by magma-filled cracks. Below we discuss these possibilities given what has been learned from recent rift zone tomographic studies and work on paleostress and recent stress directions.

3.1. Tomographic Results: Hot Mantle beneath Rifts

Tomographic experiments have been conducted across the RGR [*Davis et al.*, 1984, 1993; *Slack et al.*, 1996] the EAR [*Slack et al.*, 1994], and the BRZ [*Gao et al.*, 1994b; *Gao*, 1995] to probe the state of the mantle beneath these rifts. Travel times in the crust determined from refraction surveys were removed from the data. The remaining signals are caused by broad-scale low-velocity anomalies in the uppermost mantle beneath the rifts which extend to a much greater distance either side than the surface expression of rifting. The P wave velocity perturbations so determined are -12% for the EAR, -8% for the RGR, and -5% for the BRZ. The greatest amount of volcanism is associated with the largest velocity anomaly in East Africa, about an order of magnitude less for the RGR, and lesser amounts in the vicinity of BRZ. Attenuation measurements indicate that high-frequency P waves are preferentially absorbed in the low-velocity mantle anomalies [*Halderman and Davis*, 1991; *Slack et al.*, 1994, 1996; *Gao et al.*, 1994b].

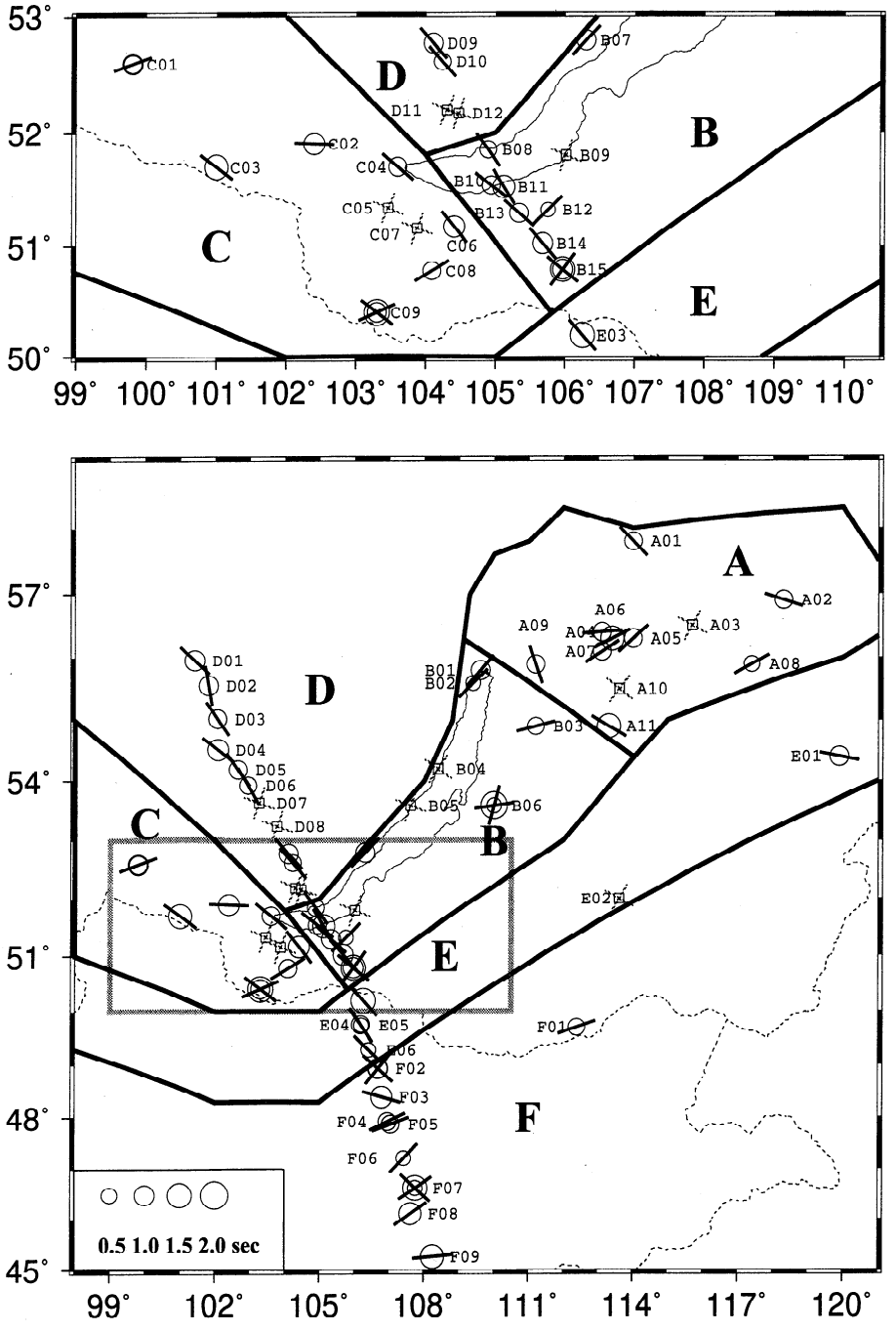

Figure 6. Maps showing *SKS* splitting results in the Baikal rift and adjacent areas. The diagram on the top is a two times enlargement of the rectangle in the bottom diagram. The line drawn through each circle gives the fast polarization direction. Those with two inconsistent results are plotted as double circles. Stations represented by squares are null measurements on which anisotropy effect cannot be clearly observed.

Using laboratory estimates of the variation of velocity and attenuation of mantle rocks with temperature by *Sato et al.* [1989], *Halderman and Davis* [1991], *Slack et al.* [1994, 1996], and *Gao et al.* [1994b] find that the tomography results can be explained if the mantle immediately beneath the rifts contains partial melt with the fraction being 2-3% beneath the EAR, possibly a fraction of a percent beneath the RGR and essentially no melt beneath the BRZ. For the BRZ the results refer to bulk averages and do not preclude the presence of pockets of melt in isolated areas corresponding to the observed patches of Cenozoic volcanism in the vicinity of the rift [*Zonenshain and Savostin*, 1981].

3.2. Relation between Paleo and Recent Stress Directions and Fast Directions

In continental rift zones the regional paleostress operating during the rifting process is inferred to be exten-

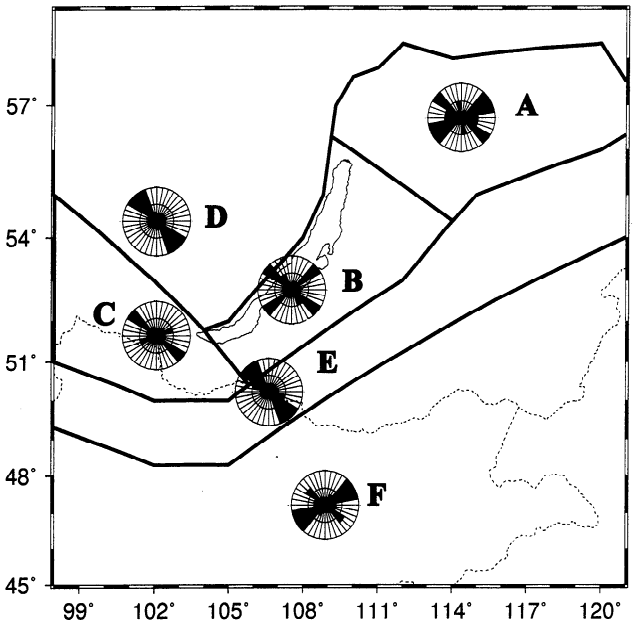

Figure 7. Rose diagrams of *SKS* fast polarization directions for each of the six areas in the BRZ and adjacent areas. Null measurements were excluded in the rose diagrams. The sector width of the rose diagrams is 20°. The two most common fast direction ranges are 40° – 80°, which is approximately parallel to the rift axis; and 120° – 160°, which is approximately rift-orthogonal.

sion in the direction of opening. For the EAR, *Bosworth et al.* [1992] use borehole breakouts and aligned Quaternary vents to show that the least principal horizontal stress (LPHS) direction is aligned approximately NW-SE in Kenya (Figure 9). In contrast, the main geological structures associated with the EAR which have developed over the last 30 Myr have formed when the LPHS was aligned E-W resulting in the N-S striking rift direction. Thus the rotation of the stress field is relatively recent event, thought to occur in the Quaternary (0.4-0.6 Ma), possibly related to the late uplift and doming of the Kenyan and Ethiopian Rifts [*Bosworth et al.*, 1992].

In a similar fashion, the stresses in the RGR and neighboring areas are thought to have undergone a clockwise rotation. Paleostress data throughout much of the western United States indicate that the LPHS underwent a transition from WSW-ENE to WNW-ESE at about 10 Myr ago, a time when Farallon subduction along the western boundary of North America had been replaced by significant development of the transform boundary of the San Andreas fault. The modern LPHS direction on the Rio Grande maintains an E-W direction, but within the transition zone between the rift and the Colorado Plateau, the LPHS is thought to be WNW-ESE (Figure 9) [*Zoback and Zoback*, 1980; *Aldrich et al.*, 1986]. The seismic tomography results

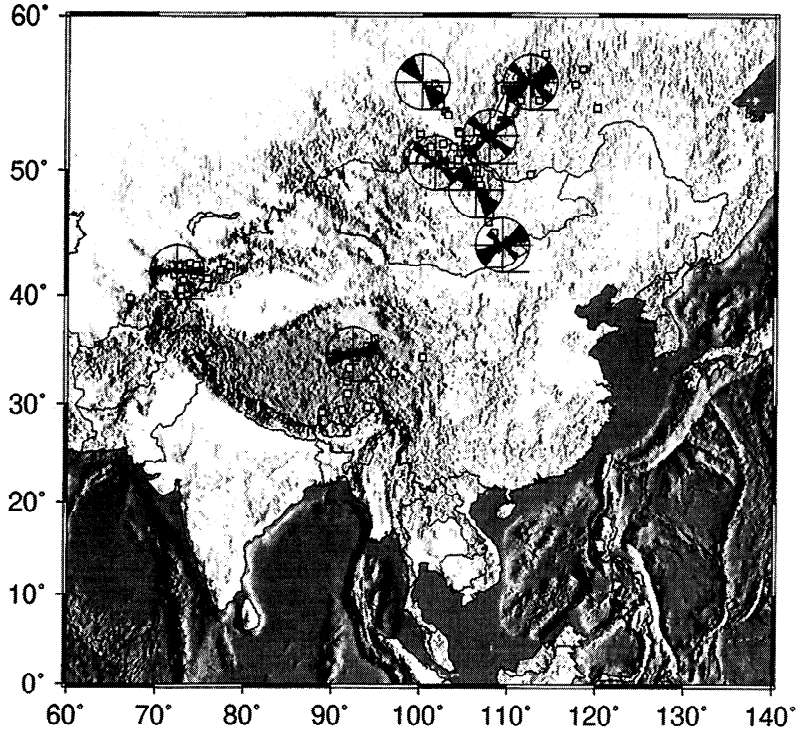

Figure 8. Rose diagrams of *SKS* splitting measurements in the zone of Tibet-Tien Shan-Mongolia-Baikal from portable seismic arrays. Stations are represented by open squares. The measurements were from the following studies: *Makeyeva et al.* [1992] (Tien Shan); *McNamara et al.* [1994] (Tibet); *Gao et al.* [1994a] and this study (Siberia-Mongolia).

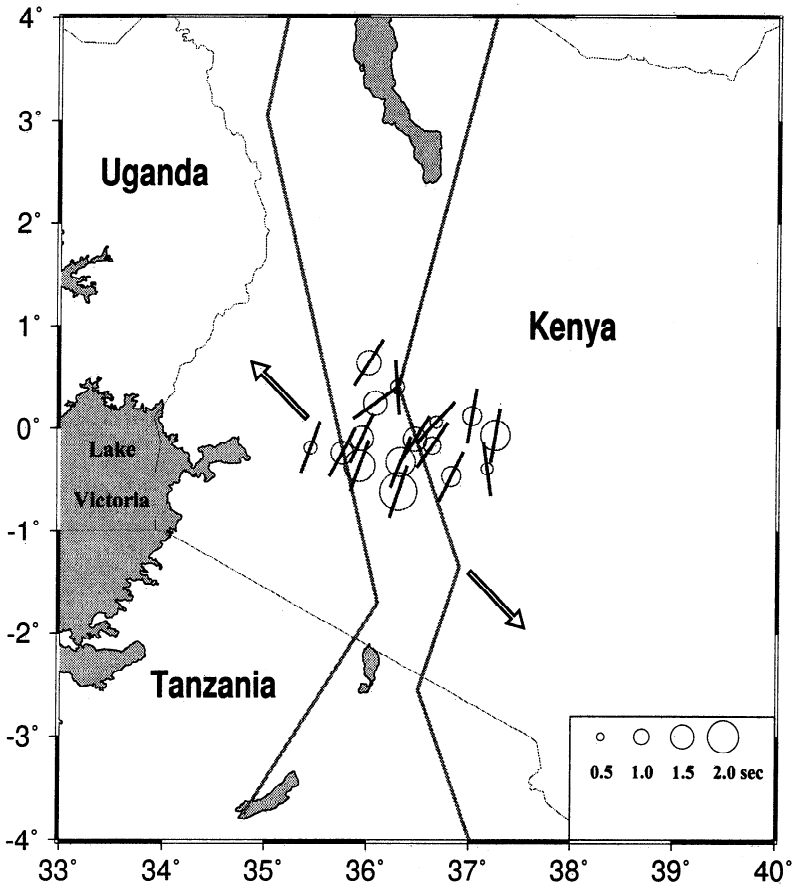

Figure 9. Maps showing *SKS* splitting results in the East African Rift [*Gao et al.*, 1994c]. Arrows represent regional stress directions [*Bosworth et al.*, 1992].

[*Slack et al.*, 1996] reveal a low-velocity body in the upper 200 km of the mantle that strikes NNE to NE, and extends from beneath the rift into the transition zone. The results were interpreted as arising from lithospheric extension in the modern (<5 Ma) LPHS direction, i.e., WNW-ESE caused by the modern stress field [*Slack et al.*, 1996]. The magnitude of the velocity anomaly and the associated attenuation in the mantle beneath the RGR were taken to imply that temperatures in the anomalous zone are close to, or even just above, the solidus. Thus *Slack et al.* [1996] conclude that it is probably the mantle source zone of the most recent volcanics that lie along this trend (e.g., the Jemez lineament).

The Baikal rift zone is a region of transtension. Figure 2 shows the regional stress fields of the BRZ [*Sherman*, 1992]. The stress fields were obtained from geological structural analysis and from earthquake focal mechanisms. *Sherman* [1992] finds that the results from the two approaches agree with each other. The regional stress pattern is also in agreement with the global stress map of *Zoback* [1992] and the subcrustal stresses that have been inferred from satellite gravity data [*Liu*, 1978, 1983]. The global stress map indicates that the LPHS lies in the direction of rift opening. However, on a more local scale, *Sherman* [1992] finds that the SW and NE regions of the rift zone are dominated by shear at the center with a transition to tensional stresses away from the center (Figure 2). The central part of the BRZ has the LPHS oriented NW-SE.

3.3. Splitting from Fossil Anisotropy, Rift-Related Mantle Flow or Magmatic Cracks?

It is possible for all these rifts that *SKS* splitting is caused by fossil anisotropy in which LPO of olivine crystals was caused by past tectonic events and has been maintained in the lithosphere ever since. Each rift zone was the site of continental convergence prior to rifting. However, mobility of olivine crystals at temperatures above 900°C is high [*Vinnik et al.*, 1992], and therefore the survival of fossil anisotropy is very unlikely in the mantle beneath the rifts, especially if the tomography interpretation is correct suggesting that the velocity anomalies are caused by mantle at temperatures close to the solidus. The tomography results indicate that the 900°C isotherm may upwarp to a depth of about 50 km beneath these rifts, as suggested by *Zorin and Osokina* [1984]. The thickness of the layer cooler than 900°C is probably too small to generate the observed splitting if all the anisotropy is fossil anisotropy.

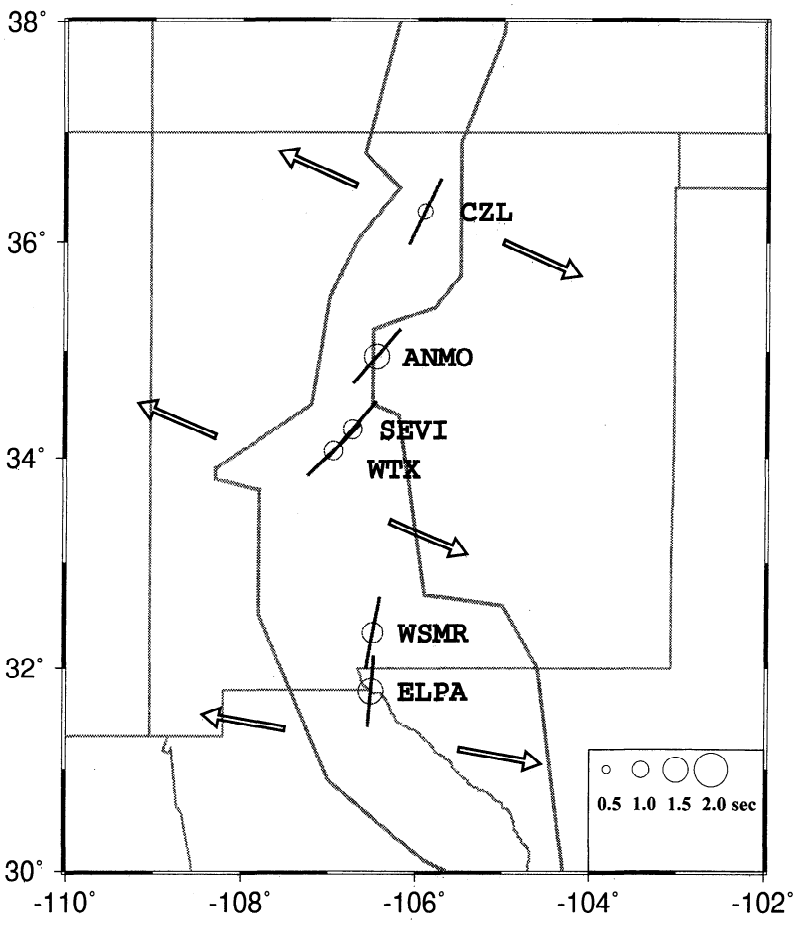

Figure 10. Maps showing *SKS* splitting results in the Rio Grande Rift [*Sandvol et al.*, 1992]. Arrows represent regional stress directions [*Zoback and Zoback*, 1980; *Aldrich et al.*, 1986].

An alternative model holds that the fast directions are caused by mantle flow. Three-dimensional small-scale convection in the mantle as suggested by *Sandvol et al.* [1992] for the RGR, or by *Makeyeva et al.* [1992] to explain anomalous directions in the Tien Shan, could give rise to rift-parallel directions. At this stage of our understanding of mantle processes beneath rifts, it is difficult to rule out this possibility.

A third model, which may be applicable in regions of hot mantle beneath rift zones, holds that aligned magmatic cracks in the mantle give rise to the fast directions. The effect on *SKS* splitting is similar to that of fluid-filled cracks in the rigid upper crust on splitting of shear waves from local earthquakes [e.g., *Leary et al.*, 1990; *Li et al.*, 1994]. Parallel vertical magmatic cracks form a transverse isotropy with rift-orthogonal axis of symmetry. The fast direction of the anisotropy is parallel to the strike of the cracks, i.e., parallel to the rift axis.

If the melt is distributed in cracks such as along grain-grain contacts or in planar dike-like regions, in a region of extension there will be a bias in the distribution of crack planes with greater numbers oriented perpendicular to the extension. It takes just a fraction of a percent of partial melt to generate the observed anisotropy, provided crack aspect ratios are high [*O'Connell and Budiansky*, 1977; *Anderson*, 1989]. This model can explain both the *P* wave delays and why the fast directions appear to be better correlated with the recent stress directions on the RGR and EAR rather than the stress directions related to the original rift events. We expect that the crack anisotropy would respond rapidly to a regional stress rotation.

In that the tomography results imply that the BRZ mantle is cooler than either the EAR or RGR, the mixture of rift-parallel and rift-orthogonal directions in the immediate vicinity of that rift may arise from a combination of LPO and oriented cracks, depending on mantle temperature. However, we add that resolving between fossil anisotropy, recent mantle flow, or aligned cracks is sufficiently difficult that favoring one over the other cannot be made with a high degree of certainty.

4. Conclusions

Observations of *SKS* splitting on the East African and Rio Grande Rifts give fast directions that are orthogonal to the least principal horizontal stress. For

Baikal, in the vicinity of the rift, the results are mixed with fast directions both orthogonal and parallel to the least principal horizontal stress. Tomography results and rift-related volcanism indicate that the mantle under the EAR is hottest and probably above the solidus, that under the Rio Grande it is near the solidus, whereas that beneath Baikal it is below the solidus. Such hot mantle may not develop LPO fabric due to annealing effects such as rotational recrystallization [*Nicolas and Poirier*, 1976]. Magmatic cracks in partially molten mantle could explain the splitting results since a bias in crack population is expected with more cracks oriented perpendicular to the LPHS. For RGR and EAR the fast directions appear to have followed the recent rotation of the stress field. This is readily explained if they are caused by a corresponding redistribution of oriented cracks. For Baikal the inferred cooler mantle may be capable of generating a fabric away from the rift zone, as observed, but in patches of hot mantle near the rift, magmatic cracks could account for the rift-parallel directions. If mantle magmatic cracks cause anisotropy in regions of extension, this can explain why observed fast directions are parallel to LPHS in compressive zones but perpendicular to it in extension zones. In the former, temperatures are lower and a fabric can develop. In the latter, temperatures are higher, possibly annealing out the fabric but causing melt pockets to form which give rise to volcanism and aligned cracks.

Acknowledgments. The field work for the Baikal rift project was done in conjunction with the late Bob Meyer, University of Wisconsin, whose presence is sorely missed. We dedicate this paper to his memory. The analog seismograms were recorded by the Baikal Seismic Network of the Russian Academy of Sciences which has been managed by a team headed by O. Masalski of IEC. We thank R. Meyer's group members, especially P. Burkholder and L. Delitsin for discussions and field cooperation. The authors are grateful to R. Girdler for helpful discussions. D. Helmberger and X. Ding at Caltech kindly provided assistance for the digitization. Most of the diagrams in this paper were produced by GMT version 3.0, a free generic mapping tool [*Wessel and Smith*, 1991]. Reviews from D. Blackman, A. Nyblade, and R. Russo are gratefully acknowledged. The study was supported by DARPA under contracts F2901-91-K-DB17 and F49620-94-1-0161 to UCLA and by ISF under grants RLN000 and RLN300 to IEC. R. Russo is thanked for assuming the role of Editor, JGR-Solid Earth, for the review process.

References

Aldrich, M. J., Jr., C. E. Chapin, and A. W. Laughlin, Stress history and tectonic development of the Rio Grande Rift, New Mexico, *J. Geophys. Res., 91,* 6199-6211, 1986.

Anderson, D. L., *Theory of the Earth,* 366 pp., Blackwell Sci., Cambridge, Mass., 1989.

Ando, M., Y. Ishikawa, and F. Yamazaki, Shear wave polarization anisotropy in the upper mantle beneath Honshu, Japan, *J. Geophys. Res., 88,* 5850-5864, 1983.

Babuska, V., and M. Cara, *Seismic Anisotropy in the Earth,* 217 pp., Kluwer Acad., Norwell, Mass., 1991.

Baker, D. W., and N. L. Carter, Seismic velocity anisotropy calculated for ultramafic minerals and aggregates, in *Flow and Fracture of Rocks,* Geophys. Monogr. Ser., Vol. 16, edited by H. C. Heard et al., pp. 157-166, AGU, Washington, D.C., 1972.

Bjarnason, I. T., C. J. Wolfe, S. C. Solomon, and G. Gudmundson, Initial results from the ICEMELT experiment–Body-wave delay times and shear-wave splitting across Iceland, *Geophys. Res. Lett., 23,* 459-462, 1996.

Bosworth, W., M. R. Strecker, and P. M. Blisniuk, Integration of east African paleostress and present-day stress data: Implications for continental stress field dynamics, *J. Geophys. Res., 97,* 11,851-11,865, 1992.

Chastel, Y. B., P. R. Dawson, H. R. Wenk, and K. Bennett, Anisotropic convection with implications for the upper mantle, *J. Geophys. Res., 98,* 17,757-17,771, 1993.

Christensen, N. I., Shear wave propagation in rocks, *Nature, 229,* 549-550, 1971.

Christensen, N. I., The magnitude, symmetry and origin of upper mantle anisotropy based on fabric analyses of ultramafic tectonites, *Geophys. J. R. Astron. Soc., 76,* 89-111, 1984.

Christensen, N. I., and S. Lundquist, Pyroxene orientation within the upper mantle, *Geol. Soc. Am. Bull., 93,* 279-288, 1982.

Christensen, N. I., and M. H. Salisbury, Seismic anisotropy in the oceanic upper mantle: Evidence from the Bay of Islands ophiolite complex, *J. Geophys. Res., 84,* 4601-4610, 1979.

Crosson, R. S., and J. -W. Lin, Voigt and Reuss prediction of anisotropic elasticity of dunite, *J. Geophys. Res., 76,* 570-578, 1971.

Davis, P. M., E. C. Parker, J. R. Evans, H. M. Iyer, and K. H. Olsen, Teleseismic deep sounding of the velocity structure beneath the Rio Grande Rift, *Field Conf. Guide B., N. M. Geol. Soc., 35th,* 29-38, 1984.

Davis, P. M., P. Slack, H. A. Dahlheim, W. V. Green, R. P. Meyer, U. Achauer, A. Glahn, and M. Granet, Teleseismic tomography of continental rift zones, in *Seismic Tomography: Theory and Practice,* edited by H. M. Iyer and H. Hirata, pp. 397-439, Chapman and Hall, New York, 1993.

Forsyth, D. W., The early structural evolution and anisotropy of the oceanic upper mantle, *Geophys. J. R. Astron. Soc., 43,* 103-162, 1975.

Fowler, C. M. R., *The Solid Earth, An Introduction to Global Geophysics,* 472 pp., Cambridge Univ. Press, New York, 1990.

Francis, T. J. G., Upper mantle structure along the axis of the Mid-Atlantic Ridge near Iceland, *Geophys. J. R. Astron. Soc., 17,* 507-520, 1969.

Fuchs, K., Seismic anisotropy of the subcrustal lithosphere as evidence for dynamical processes in the upper mantle, *Geophys. J. R. Astron. Soc., 49,* 167-179, 1977.

Gao, S., Seismic evidence for small-scale mantle convection under the Baikal rift zone, Siberia, Ph.D. thesis, 221 pp., Univ. of Calif., Los Angeles, 1995.

Gao, S., P. M. Davis, H. Liu, P. D. Slack, Y. A. Zorin, V. V. Mordvinova, V. M. Kozhevnikov, and R. P. Meyer, Seismic anisotropy and mantle flow beneath the Baikal rift zone, *Nature, 371,* 149-151, 1994a.

Gao, S., P. M. Davis, H. Liu, P. Slack, Y. A. Zorin, N. A. Logatchev, M. Kogan, P. Burkholder, and R. P. Meyer, Asymmetric upwarp of the asthenosphere beneath the Baikal rift zone, Siberia, *J. Geophys. Res., 99,* 15,319-15,330, 1994b.

Gao, S., P. M. Davis, H. Liu, P. D. Slack, Y. A. Zorin, V. V. Mordvinova, V. M. Kozhevnikov, and R. P. Meyer, Seismic Anisotropy beneath the Baikal and Kenya rift zones (abstract), *Eos Trans. AGU, 75*(3), West. Pac. Geophys. Meet. Suppl., 67, 1994c.

Halderman, T. P., and P. M. Davis, Q_p beneath the Rio Grande and East African Rift zones, *J. Geophys. Res., 96,* 10,113-10,128, 1991.

Hess, H. H., Seismic anisotropy of the upper most mantle under oceans, *Nature, 203,* 629-631, 1964.

Humphrey, N., and D. Helmberger, *NXSCAN,* IRIS Data Manage. Cent., Seattle, Wash., 1993.

Karato, S., Seismic anisotropy: Mechanisms and tectonic implications, in *Rheology of solids and of the Earth,* edited by S. Karato and M. Toriumi, pp. 393-422, Oxford Univ. Press, Oxford, 1989.

Kendall, J. M., Teleseismic arrivals at a mid-ocean ridge: Effects of mantle melt and anisotropy, *Geophys. Res. Lett.,* 21, 301-304, 1994.

Kind, R., G. L. Kosarev, L. I. Makeyeva, and L. P. Vinnik, Observations of laterally inhomogeneous anisotropy in the continental lithosphere, *Nature, 318,* 358-361, 1985.

Leary, P. C., S. Crampin, and T. V. McEvilly, Seismic fracture anisotropy in the Earth's crust: An overview, *J. Geophys. Res., 95,* 11,105-11,114, 1990.

Li, Y. G., T. L. Teng, and T. L. Henyey, Shear-wave splitting observations in the northern Los Angeles Basin, southern California, *Bull. Seismol. Soc. Am., 84,* 307-323, 1994.

Liu, H. S., Mantle convection pattern and subcrustal stress field under Asia, *Phys. Earth Planet. Inter., 16,* 247-256, 1978.

Liu, H. S., Geodynamics of the Baikal-Stanovoy seismic belt, *Phys. Earth Planet. Inter., 31,* 77-82, 1983.

Liu, H., P. M. Davis, and S. Gao, *SKS* splitting beneath southern California, *Geophys. Res. Lett., 22,* 767-770, 1995.

Makeyeva, L. I., L. P. Vinnik, and S. W. Roecker., Shear-wave splitting and small-scale convection in the continental upper mantle, *Nature, 358,* 144-147, 1992.

McKenzie, D., Finite deformation during fluid flow, *Geophys. J. R. Astron. Soc., 58,* 689-715, 1979.

McNamara, D. E., T. J. Owens, P. G. Silver, and F. T. Wu, Shear wave anisotropy beneath the Tibetan Plateau, *J. Geophys. Res., 99,* 13,655-13,665, 1994.

Mercier, J. C. C. Olivine and pyroxenes, in *Preferred Orientation in Deformed Metals and Rocks: An Introduction to Modern Texture Analysis,* edited by H. Wenk, pp. 407-430, Acad. Press, Orlando, Flor., 1985.

Montagner, J., and T. Tanimoto, Global upper mantle tomography of seismic velocities and anisotropies, *J. Geophys. Res., 96,* 20,337-20,351, 1991.

Nicolas, A., and N. I. Christensen, Formation of anisotropy in upper mantle peridotites: A review, *Geodynamics Ser., 16,* 111-123, 1987.

Nicolas, A., F. Boudier, and A. M. Boullier, Mechanisms of flow in naturally and experimentally deformed peridotites, *Am. J. Sci., 273,* 853-876, 1973.

Nicolas, A., and J. P. Poirier, *Crystalline Plasticity and Solid State Flow in Metamorphic Rocks,* 444 pp., John Wiley & Sons, London, 1976.

O'Connell, R. J., and B. Budiansky, Viscoelastic properties of fluid-saturated cracked solids, *J. Geophys. Res., 82,* 5719-5735, 1977.

Olsen, K. H., and P. Morgan, Introduction: Progress in understanding continental rifts, in *Continental Rifts: Evolution, Structure and Tectonics,* edited by K. H. Olsen, pp. 3-26, Elsevier, New York, 1995.

Peselnick, L., A. Nicolas, and P. R. Stevenson, Velocity anisotropy in a mantle peridotite from the Ivrea Zone: Application to upper mantle anisotropy, *J. Geophys. Res., 79,* 1175-1182, 1974.

Raitt, R. W., G. G. Shor Jr., T. J. G. Francis, and G. B. Morris, Anisotropy of the Pacific upper mantle, *J. Geophys. Res., 74,* 3095-3109, 1969.

Ribe, N. M., On the relation between seismic anisotropy and finite strain, *J. Geophys. Res., 97,* 8737-8747, 1992.

Ribe, N. M., and Y. Yu, A theory for plastic deformation and textural evolution of olivine polycrystals, *J. Geophys. Res., 96,* 8325-8355, 1991.

Sandvol, E., J. Ni, S. Ozalaybey, and J. Schlue, Shear-wave splitting in the Rio Grande Rift, *Geophys. Res. Lett., 19,* 2337-2340, 1992.

Sato, H., I. S. Sacks, and T. Murase, The use of laboratory velocity data for estimating temperature and partial melt fraction in the low-velocity zone: Comparison with heat flow and electrical conductivity studies, *J. Geophys. Res., 94,* 5689-5704, 1989.

Savage, M. K., and P. G. Silver, Mantle deformation and tectonics: Constraints from seismic anisotropy in the western United States, *Phys. Earth Planet. Inter., 78,* 207-227, 1993.

Savage, M. K., P. G. Silver, and R. P. Meyer, Observations of teleseismic shear-wave splitting in the basin range from portable and permanent stations, *Geophys. Res. Lett., 17,* 21-24, 1990.

Sherman, S. I., Faults and tectonic stresses of the Baikal rift zone, *Tectonophysics, 208,* 297-307, 1992.

Silver, P. G., Seismic anisotropy beneath the continents–Probing the depths of geology, *Annu. Rev. Earth Planet. Sci., 24,* 385-432, 1996.

Silver, P. G., and W. W. Chan, Implications for continental structure and evolution from seismic anisotropy, *Nature, 335,* 34-39, 1988.

Silver, P. G., and W. W. Chan, Shear wave splitting and subcontinental mantle deformation, *J. Geophys. Res., 96,* 16,429-16,454, 1991.

Silver, P. G., and S. Kaneshima, Constraints of mantle anisotropy beneath Precambrian North America from a transportable teleseismic experiment, *Geophys. Res. Lett., 20,* 1131-1134, 1993.

Slack, P. D., P. M. Davis, H. A. Dahlheim, A. Glahn, J. R. R. Ritter, W. V. Green, P. K. H. Maguire, and R. P. Meyer, Attenuation and velocity of *P*-waves in the mantle beneath the East African Rift, Kenya, *Tectonophysics, 236,* 331-358, 1994.

Slack, P. D., P. M. Davis, W. S. Baldridge, K. H. Olsen, A. Glahn, U. Achauer, and W. Spence, The upper mantle structure of the central Rio Grande Rift region from teleseismic *P* and *S* wave travel time delays and attenuation, *J. Geophys. Res., 101,* 16,003-16,023, 1996.

Tanimoto, T., and D. L. Anderson, Lateral heterogeneity and azimuthal anisotropy of the upper mantle: Love and Rayleigh waves 100-250 s, *J. Geophys. Res., 90,* 1842-1858, 1985.

Turcotte, D. L., and G. Schubert, *Geodynamics, Applications of continuum physics to geological problems,* John Wiley, New York, 1982.

Verma, R. K., Elasticity of several high-density crystals, *J. Geophys. Res., 65,* 757-766, 1960.

Vinnik, L. P., V. Farra, and B. Romanowicz, Azimuthal anisotropy in the Earth from observations of *SKS* at Geoscope and NARS broadband stations, *Bull. Seismol. Soc. Am., 79,* 1542-1558, 1989.

Vinnik, L. P., L. I. Makeyeva, A. Milev, and A. Y. Usenko, Global patterns of azimuthal anisotropy and deformations in the continental mantle, *Geophys. J. Int., 111,* 433-447, 1992.

Wessel, P., and W. H. F. Smith, Free software helps map and display data, *Eos Trans. AGU, 72,* 441, 445-446, 1991.

Zoback, M. L., First- and second-order patterns of stress in the lithosphere: The World Stress Map Project, *J. Geophys. Res., 97,* 11,703-11,728, 1992.

Zoback, M. L., and M. D. Zoback, State of stress in the

conterminous United States, *J. Geophys. Res., 85,* 6113-6156, 1980.

Zonenshain, L. P., and L. A. Savostin, Geodynamics of the Baikal rift zone and plate tectonics of Asia, *Tectonophysics, 76,* 1-45, 1981.

Zorin, Y. A., and S. V. Osokina, Model of the transient temperature fields of the Baikal rift lithosphere, *Tectonophysics, 103,* 193-204, 1984.

P. M. Davis, H. Liu, P. D. Slack, and A. W. Rigor, Department of Earth and Space Sciences, University of California, Los Angeles, CA 90095. (e-mail: pdavis@ess.ucla.edu; hliu@dtm.ciw.edu; pslack@ess.ucla.edu; arigor@ess.ucla.edu)

S.Gao, Department of Terrestrial Magnetism, Carnegie Institution of Washington, 5241 Broad Branch Road, N.W., Washington, DC 20015. (e-mail: sgao@dtm.ciw.edu)

Y. A. Zorin, V. V. Mordvinova, V. M. Kozhevnikov, and N. A. Logatchev, Institute of the Earth's Crust, Siberian Branch, Russian Academy of Sciences, 128 Lermontov Street, Irkutsk 664 033, Russia. (e-mail: zorin@crust.irkutsk.su)

(Received December 3, 1996; revised May 30, 1997; accepted June 24, 1997.)